Neuro-Oncology

Neuro-Oncology 17(3), 457–465, 2015
doi:10.1093/neuonc/nou230
Advance Access date 30 November 2014

Delayed contrast extravasation MRI: a new paradigm in neuro-oncology

Leor Zach, David Guez, David Last, Dianne Daniels, Yuval Grober, Ouzi Nissim, Chen Hoffmann, Dvora Nass, Alisa Talianski, Roberto Spiegelmann, Galia Tsarfaty, Sharona Salomon, Moshe Hadani, Andrew Kanner, Deborah T. Blumenthal, Felix Bukstein, Michal Yalon, Jacob Zauberman, Jonathan Roth, Yigal Shoshan, Evgeniya Fridman, Marc Wygoda, Dror Limon, Tzahala Tzuk, Zvi R. Cohen, and Yael Mardor

Oncology Institute (L.Z., A.T.); Advanced Technology Center (D.G., D.L., D.D., S.S., Y.M.); Neurosurgery Department (Y.G., O.N., R.S., M.H., J.Z., Z.R.C.); Radiology Institute (C.H., G.T.); Pathology Institute (D.N.); Pediatric Hemato-Oncology Department, Sheba Medical Center, Ramat-Gan, Israel (M.Y.); Sackler Faculty of Medicine, Tel-Aviv University, Tel-Aviv, Israel (L.Z., D.D., C.H., R.S., G.T., M.Y., Z.R.C., Y.M.); Neuro-Oncology Service (D.T.B., F.B.); Neurosurgery Department, Tel-Aviv Medical Center, Tel-Aviv, Israel (A.K., J.R.); Neuro-Oncology Service (E.F., M.W.); Neurosurgery Department, Hadassah Medical Center, Jerusalem, Israel (Y.S.); Oncology Institute, Davidoff Center, Rabin Medical Center, Petach Tikva, Israel (D.L.); Neuro-Oncology Service, Rambam Medical Center, Haifa, Israel (T.T.)

Corresponding Author: Yael Mardor, PhD, The Advanced Technology Center, Sheba Medical Center, Tel-Hashomer 52621, Israel (yael.mardor@sheba.health.gov.il).

Background. Conventional magnetic resonance imaging (MRI) is unable to differentiate tumor/nontumor enhancing tissues. We have applied delayed-contrast MRI for calculating high resolution treatment response assessment maps (TRAMs) clearly differentiating tumor/nontumor tissues in brain tumor patients.

Methods. One hundred and fifty patients with primary/metastatic tumors were recruited and scanned by delayed-contrast MRI and perfusion MRI. Of those, 47 patients underwent resection during their participation in the study. Region of interest/threshold analysis was performed on the TRAMs and on relative cerebral blood volume maps, and correlation with histology was studied. Relative cerebral blood volume was also assessed by the study neuroradiologist.

Results. Histological validation confirmed that regions of contrast agent clearance in the TRAMs >1 h post contrast injection represent active tumor, while regions of contrast accumulation represent nontumor tissues with 100% sensitivity and 92% positive predictive value to active tumor. Significant correlation was found between tumor burden in the TRAMs and histology in a subgroup of lesions resected en bloc ($r^2 = 0.90$, $P < .0001$). Relative cerebral blood volume yielded sensitivity/positive predictive values of 51%/96% and there was no correlation with tumor burden. The feasibility of applying the TRAMs for differentiating progression from treatment effects, depicting tumor within hemorrhages, and detecting residual tumor postsurgery is demonstrated.

Conclusions. The TRAMs present a novel model-independent approach providing efficient separation between tumor/nontumor tissues by adding a short MRI scan >1 h post contrast injection. The methodology uses robust acquisition sequences, providing high resolution and easy to interpret maps with minimal sensitivity to susceptibility artifacts. The presented results provide histological validation of the TRAMs and demonstrate their potential contribution to the management of brain tumor patients.

Keywords: brain metastases, brain tumor, delayed-contrast MRI, pseudoprogression, radiation necrosis.

Previous studies suggest that 14%–30% of glioblastoma multiforme (GBM) patients experience treatment effects in the first few months after treatment.[1–8] Similarly, 5%–24% of patients with brain metastases experience treatment effects at various durations following radiation-based therapies.[9] These treatment-induced changes, often termed pseudoprogression/radiation necrosis, are depicted as increasing volumes of contrast-enhancing lesions on MRI, mimicking progression. Treatment decisions, such as whether to operate on a patient with radiographic deterioration, continue current treatment, or change treatment, is a daily struggle involving interdisciplinary teams of neurosurgeons, neuro-oncologists, and neuroradiologists who are often unable to reach unanimous interpretation of the patient's status.

Received 17 April 2014; accepted 8 August 2014

Despite the questionable value of histological findings in biopsies/resections performed posttreatment,[10] quantification of tumor burden within surgical material appears to provide prognostic value.[11–13] Therefore, reliable noninvasive quantification of tumor burden may be applied for improving patient management.[14–18]

MR spectroscopy provides information on the tissue metabolism and is being extensively evaluated toward distinction of progression from radiation necrosis.[19] FDG (2-fluoro-2-deoxy-D-glucose)-PET has been shown to be useful in differentiating radiation necrosis from recurrence, but it has low sensitivity/specificity in the brain.[20] There is limited but increasing evidence that PET with amino acid tracers may be of benefit.[21]

Perfusion-weighted MRI is the most studied methodology in this context, using dynamic contrast-enhanced MRI and dynamic susceptibility-weighted contrast (DSC) MRI.[21–23] Treatment effects typically show decreased relative cerebral blood volume (rCBV), whereas tumor shows high rCBV.[24–31] Still, most of these studies show significant overlap between the 2 conditions. In addition, fast acquisition techniques provide low spatial resolution and are subject to susceptibility artifacts.

We have recently presented preliminary results in which delayed contrast MRI was used to calculate high resolution maps showing clear differentiation between tumor/nontumor tissues in brain tumor patients.[32] This methodology is based on MRIs acquired 3 and 75 min on average after a conventional injection of contrast agent. The MRIs are then processed to provide treatment response assessment maps (TRAMs). Blue/tumor regions in the TRAMs represent efficient clearance of contrast from the tissue (delayed signal < early signal), while red/nontumor regions in the TRAMs represent contrast accumulation (delayed signal > early signal). When comparing the presurgical TRAMs with histological samples acquired from 20 patients with primary/metastatic brain tumors, we found that blue regions in the maps consisted of morphologically active tumor, while red regions consisted of nontumor abnormal tissues. In addition, we demonstrated that the common vessels morphology in the blue region was undamaged vessel lumens, while vessels in the red regions presented different stages of vessel necrosis. Therefore, one explanation for the difference between the 2 populations may be that vessels in blue/tumor regions provide efficient contrast clearance from the tissue, while the damaged lumens in the red/treatment-effects regions are unable to clear the accumulating contrast, resulting in contrast accumulation.

Below we present the full results of this study, including histological validation of the TRAMs and comparison with DSC-MRI.

Materials and Methods

Patients and Treatment

The study was conducted after approval of the local ethics committee at Sheba Medical Center. Written informed consent was obtained from all patients.

The study was designed to assess the application of delayed contrast MRI to follow patients with brain tumors posttreatment. The primary endpoint was to establish the application of the TRAMs for differentiating active disease from treatment effects via histology; secondary endpoints were to determine patterns of response, progression, pseudoprogression, and radiation necrosis using the TRAMs and to assess possible applications of the TRAMs for clinical decision making.

Inclusion criteria were brain space–occupying lesions immediately prior to or posttreatment and patient age >18 years. Exclusion criteria were World Health Organization performance status ≤3 and contraindications to MRI. Patients were recruited either for follow-up (to study the evolution pattern of response, progression, treatment effects, and radiation necrosis) or with a question of progression versus treatment effects. Since progression or treatment effects may recur more than once, patients were followed on study until they decided to retire or were unable to undergo the MRI exams.

One hundred and fifty patients with primary/metastatic brain tumors were recruited. Sixty-six were females, and the mean age at recruitment was 53.2 ± 1.2 years (range, 18.1–83.1); numbers of cases were 46 GBM, 8 anaplastic astrocytomas, 5 oligodendrogliomas, 1 anaplastic oligodendroglioma, 1 anaplastic oligoastrocytoma, 1 anaplastic meningioma, 1 low-grade oligodendroglioma, 2 low-grade astrocytomas, 2 chordomas, 1 arteriovenous malformation, 27 breast cancers, 1 male breast cancer, 24 non–small cell lung cancers (NSCLCs), 17 malignant melanomas, 2 ovarian cancers, 2 adenocarcinomas of unknown source, 1 yolk sac carcinoma, 1 colon cancer, 2 adenoid cystic carcinomas, 1 petroclival meningioma, 2 atypical meningiomas, and 2 head and neck cancers. Additional information regarding the patients and treatments is detailed in Supplementary File 1.

MRI Data Acquisition

Patients were scanned by MRI immediately following recruitment and every 2 months thereafter or earlier according to their clinical condition. The MRIs were acquired using 1.5T/3T General Electric MRI systems and included DSC-MRI, fast spin echo T2-weighted MRI, T2 fluid attenuated inversion recovery, and echo-planar diffusion-weighted MRI. High resolution spin echo T1-weighted (T1) MRIs were acquired before, 3.0 ± 0.2 min after (immediately after the DSC-MRI sequence), and 74.5 ± 0.2 min after contrast injection (hereafter referred to as the 3 and 75 min time points). Patients were scanned up to ~30 min after contrast injection (the hospital standard brain tumor protocol), were taken out of the MRI system, and were then asked to return for a short scan ~75 min after contrast injection.

T1-MRIs were acquired with echo time of 22 ms and repetition time of 240 ms, field of view 26×19.5 cm, 5/0.5 mm slice thickness, and 512×512 pixels. DSC-MRIs were acquired with echo time of 50 ms and repetition time of 2000 ms, flip angle 70 degrees, field of view 26×19.5 cm, 5/0.5 mm slice thickness, and 96×128 pixels.

A standard single dose (0.2 mL/kg, 0.1 mmol/kg) of gadolinium DOTA (1,4,7,10-tetraazacyclododecane-1,4,7,10-tetraacetic acid 0.5 mmol/mL; Dotarem, Guerbet) was injected intravenously using an automatic injection system 6 s after starting the DSC-MRI sequence. No preload contrast dose was administered.

MRI Data Analysis

All image analysis was performed using MatLab version R2010a (MathWorks). The overall goal of the analysis was to obtain

subtraction maps, in which T1-MRIs acquired 3 min postcontrast were subtracted from T1-MRIs acquired 75 min postcontrast. These maps depict spatial distribution of contrast accumulation/clearance. For example, in the case of normal blood vessels, due to contrast clearance from the blood, the signal decreases with time; therefore, the subtraction maps show negative values (blue in the maps). In the case of contrast accumulation, the maps show positive values (red).

In order to increase the sensitivity to small changes, it was essential to perform image preprocessing consisting of corrections for intensity variations and whole body image registration as previously described.[32] In short, an intensity correction was performed on each image by calculating intensity variation maps, consisting of large-scale intensity variations, and subtracting them from the original images. Rigid body registration was performed using a least-squares approach and 6-parameter spatial transformation with the Statistical Parametric Mapping 8 MatLab routine (academic software kit by Wellcome Trust Centre for Neuroimaging). Due to magnetic distortions, local/elastic registration was also performed by dividing each slice to a grid of 20×20 mm volumes. Each volume was allowed to move freely in *x-y-z* until the sum of the absolute values of the intensity difference between the 2 time points reached a minimum. The resulting three 3D translation matrices were smoothed using circular smearing and interpolated to obtain translation values per pixel. These high resolution matrices were then applied to register T1-MRIs of the second time point to the location of the first time point. Finally, TRAMs were calculated by voxel-by-voxel subtraction of the early images from the late images.

Enhancing volume regions of interest (ROIs) were calculated by threshold analysis as detailed in Supplementary File 1.

RCBV maps were calculated from the DSC-MRIs with a leakage correction using commercially available software (FuncTools $5 \times 2.1.08$, GE Healthcare). These maps were normalized to the average rCBV value of an ROI chosen in contralateral normal-appearing white matter.[26] The average value of rCBV in the enhancing lesion ROI was then calculated by registering the T1-MRIs to the rCBV maps and copying the enhancing ROIs from the T1-MRIs to the rCBV maps. High rCBV was defined as rCBV > 1.8 based on previously published thresholds.[13,26,33] The volume of high rCBV was therefore defined as the volume of all pixels in the ROI with values >1.8. The enhancing ROI was then flipped over the midline to calculate the same parameters in the contralateral hemisphere.

Due to the inherent low resolution, distortion, and masking effects of normal-brain vascular regions (such as the midline and gray matter) in rCBV maps, in addition to the ROI analysis, rCBV was assessed by the study neuroradiologist (C.H.) as routinely performed in our hospital. The study neuroradiologist reviewed the DSC-MRI data of all patients, blinded to the TRAMs, and categorized the lesion rCBV as follows:

(1) **High rCBV:** at least part of the lesion can be delineated from gray matter anatomy (normally enhanced on rCBV maps) and demonstrates, at least in part, similar/higher rCBV than gray matter. High rCBV, as defined here, is used at the Sheba Medical Center to determine active tumor based on DSC-MRI.
(2) **Moderate rCBV:** at least part of the lesion can be delineated from gray matter anatomy and demonstrates moderate rCBV (lower than gray matter but still enhancing).
(3) **Low rCBV:** demonstrates either very low signal or is completely undetectable on rCBV maps.

Histology

Comparison between the presurgical maps and histology was previously reported for the first 22 lesions obtained from 20 patients with brain tumors.[32] These data are merged here with the histological evaluation of an additional 29 lesions obtained from 27 patients. Conventional pathological reports were prepared by the hospital neuropathologist according to the routine hospital protocol. In addition, preplanned biopsied samples were obtained and marked by the neurosurgeon during resection. Histological evaluation consisted of blinded pathological reports and nonblinded histological evaluation of the biopsies/en-bloc samples.

Morphologically active tumor was defined as demonstrating one or more of the following: hypercellularity with small cells, mitoses, high Ki67, pseudopalisading necrosis, vascular proliferation. Nontumor abnormal tissue, including treatment effects, was defined as demonstrating one or more of the following: radiation changes including large, widely spaced atypical astrocytes, blood vessel hyalinization, fibrinoid material in vessels, proliferating small vessels, or nonpalisading tumor necrosis.

In order to calculate the correlation between the presurgical TRAMs and histological tumor burden, the percentage of active tumor was calculated from the histological samples by threshold analysis. The threshold was determined by the study neuropathologist (D.N., blinded to the TRAMs). Additional information can be found in Supplementary File 1.

Results

Treatment Response Assessment Maps

As previously described,[32] 2 primary enhancement patterns were found in the TRAMs—one characterized by contrast accumulation at the delayed time point, resulting in a positive signal in the TRAMs (red/nontumor), and the other characterized by contrast clearance at the delayed time point (blue/tumor). Examples are shown in Fig. 1.

Histological Validation of Treatment Response Assessment Maps

Histological evaluations of 51 lesions resected from 47 patients were compared with the presurgical maps. Details regarding the biopsies, samples resected en bloc, and whole lesion information are listed in Table 1. Detailed histological assessments of all the samples, including those previously described,[32] are listed in Supplementary Table S1.

Based on the blinded histological reports, complete agreement between the presurgical TRAMs and histology was found in 47 of 51 resected lesions, suggesting sensitivity and positive predictive value (PPV) to active tumor of 100% and 92%, respectively. When separating primary from metastatic tumors, we found the sensitivity/PPV to primary brain tumors to be 100%/96% and to brain metastases 100%/89%.

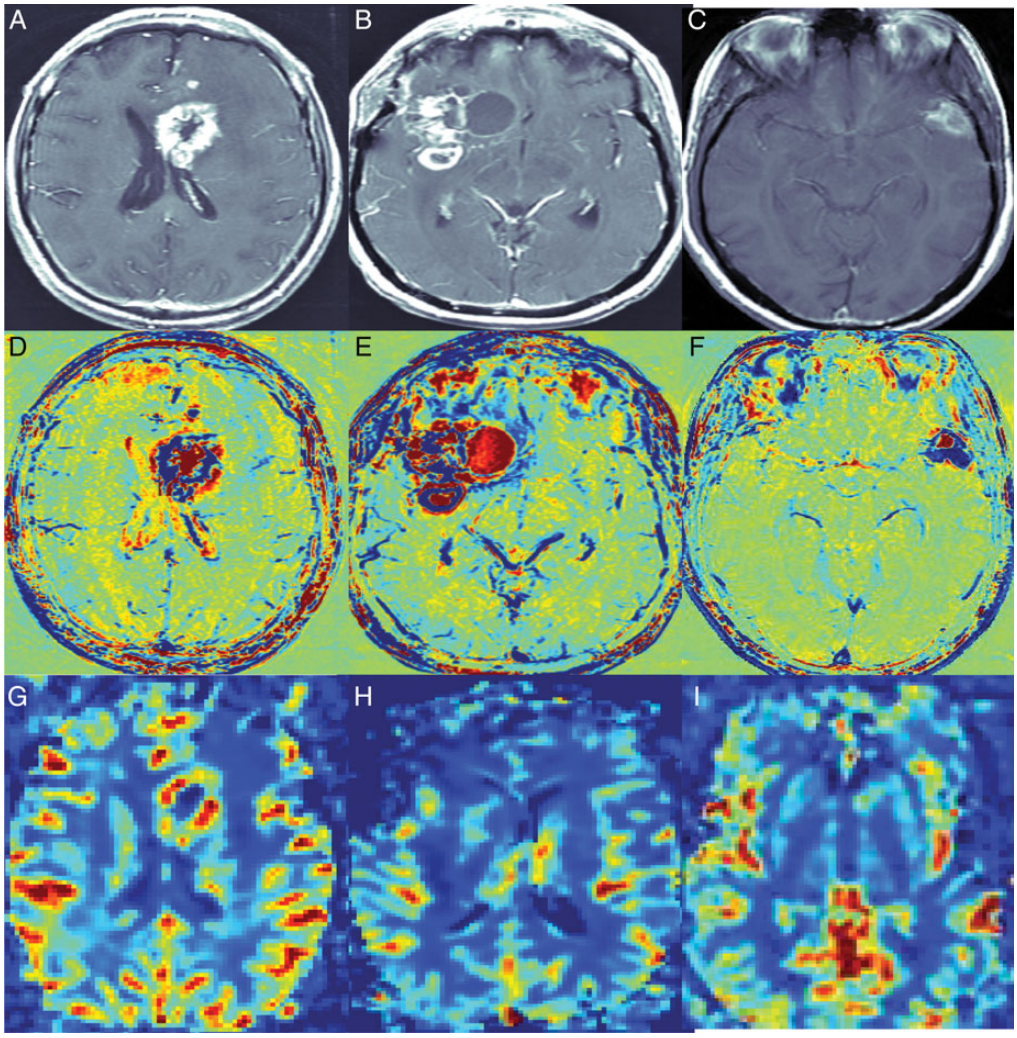

Fig. 1. Contrast-enhanced MRI (A–C), the calculated TRAMs (D–F), and rCBV maps (G–I) of GBM patients 3 weeks (A, D, and G) and 3 months (B, E, and H) postchemoradiation and a patient with a malignant melanoma brain metastasis (C, F, and I) 2 months post stereotactic radiosurgery. The 3 lesions, all showing a blue/tumor component in the TRAMs, were categorized by the study neuroradiologist as having high (G), moderate (H), and low rCBV (I).

The addition of the nonblinded data (62 biopsied samples and 8 en bloc samples) resulted in sensitivity/PPV of 99%/95%. Disagreements between the TRAMs and histology were found in 4 cases. In 3 cases of brain metastases, the presurgical maps showed ~85% red and ~15% blue, while no tumor was found in histology. Still, a blue/tumor rim surrounding the surgery site appeared 1–4 months postsurgery in all 3 patients, suggesting residual/recurrent tumor. The fourth case was of a GBM patient 4 months postsurgery followed by 6 weeks of chemoradiation and one course of temozolomide. In this case the TRAMs showed a blue/tumor volume of 3.3 mL at recruitment and 12.8 mL 2 months later, prior to surgery. Despite the rapid growth in blue/tumor volume, histology determined the tumor to be quiescent. Five weeks postsurgery, a thick blue rim was depicted surrounding the surgery site, suggesting recurrent tumor. The patient started treatment with temozolomide but 2 months later progressed and switched to bevacizumab.

The correlation between the blue percentage in the enhancing ROIs of the presurgical TRAMs and the tumor percentage in histology was calculated for 12 lesions in which the percentage of active tumor in histology could be assessed: 8 en bloc samples, 3 samples that showed no tumor in histology, and 1 sample estimated by the neuropathologist to consist of 5% active tumor. Figure 2 shows examples of NSCLC and yolk sac carcinoma metastases resected en bloc. The correlation calculated for the 12 samples was found to be significant: $r^2 = 0.90$, $P < .0001$ (Pearson correlation). Only 8 of the 12 samples had rCBV data available; therefore, the correlation was recalculated for these 8 samples, resulting in $r^2 = 0.93$, $P < .0001$.

Histological Validation of Relative Cerebral Blood Volume

Presurgical rCBV data were available for 46 of the 51 resected lesions. Using ROI analysis, high rCBV was found in 45 of the 46

Table 1. Detailed summary of the histological samples

Sample Type	# of Samples	Total # of Patients	# of Primary Tumors	# of Metastatic Tumors	Active Tumor Found in Histology
Total number of resected lesions	51	47	21	26	47 yes, 4 no
Lesion resected en bloc	8	8	1	7	Yes
Lesions resected without biopsies	29	27	6	21	25 yes, 4 no
Biopsies	46 (45 taken from blue regions; 1 taken from red region)	21	15	6	Yes
Biopsies	16 taken from red regions	12	8	4	No

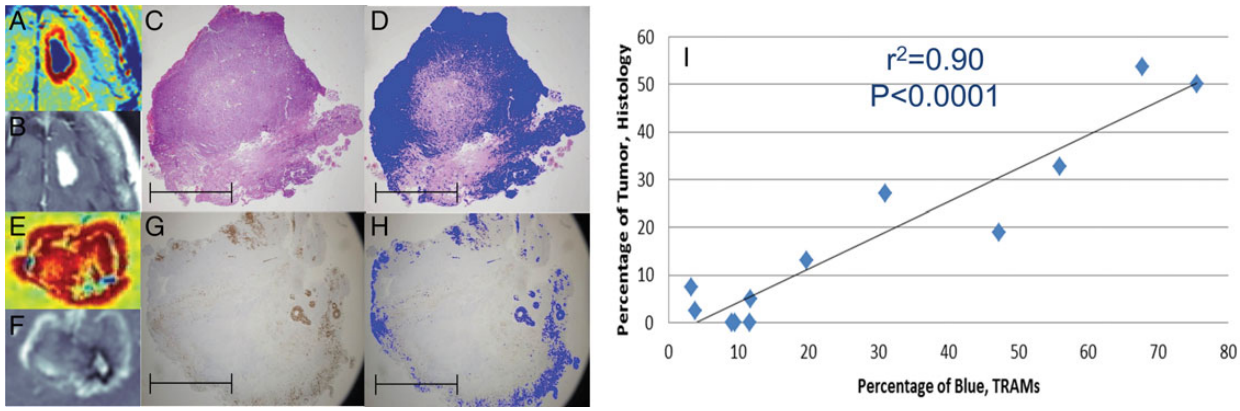

Fig. 2. Correlation between the percent of blue regions in the presurgical TRAMs and the percent of active tumor in histology. Shown are examples of an NSCLC lesion (A–D) stained by hematoxylin and eosin and a yolk sac carcinoma lesion (E–H) stained by keratin, resected en bloc. Scale bar, 5 mm. For each example, the calculated TRAMs (A and E), contrast-enhanced T1-weighted MRIs (B and F), and histological samples without (C and G) and with (D and H) a threshold (blue) marking the regions of active tumor are shown. The plot (I) shows significant correlation between the TRAMs and histology.

samples, resulting in sensitivity and PPV to active tumor of 100% and 98%, respectively.

We believe that ROI analysis, as performed here, may be misleading due to masking by high rCBV of normal brain anatomy, as demonstrated in the examples of Fig. 3. In order to study this masking effect, we performed additional ROI analysis on the cohort of 46 resected patients who had DSC-MRI data available. The average volume of high rCBV was calculated in the enhancing lesion ROIs and in contralateral ROIs of the same shape/size for all patients. The average volume of high rCBV in the enhancing ROIs was 12.1 ± 2.4 mL and in the contralateral ROIs 12.3 ± 2.1 mL. There was no significant difference between the 2 ROI groups ($P < .98$, 2-tailed paired *t*-test). Average rCBV in the enhancing ROIs was 2.4 ± 0.2 and in the contralateral ROIs 2.3 ± 0.2. There was no significant difference between these 2 groups either ($P < .24$, 2-tailed paired *t*-test). In addition, the ratio between the volume of high rCBV in the enhancing ROI and in the contralateral ROI was calculated for all patients. The average value of this ratio was 1.1 ± 0.1. These results suggest that this method of ROI analysis is heavily masked by normal brain vascular anatomy.

Similar analysis was performed for the TRAMs. The average blue volume in the enhancing ROIs was 11.1 ± 2.2 mL, while in the contralateral ROIs it was 1.7 ± 0.4 mL. Blue volumes in the contralateral regions are attributed to blood vessels. The difference between the blue volumes in the enhancing ROIs and in the contralateral ROIs was found to be significant ($P < .0001$, 2-tailed paired *t*-test). Similarly to the rCBV analysis, we calculated the ratio between the blue volumes in the enhancing ROI and in the contralateral ROI for all patients. The average value of this ratio was 12.0 ± 3.7.

Based on the above analysis, we conclude that high rCBV in the enhancing lesion, calculated using the ROI analysis presented here, may be a reliable indication for tumor only in cases where the tumor location is isolated from gray matter, as in the case of Fig. 3A–E. For this reason we also applied the clinical approach and recalculated sensitivity/PPV using the neuroradiologist's determination of high rCBV, resulting in 51%/96%. When separating primary from metastatic tumors, we found the sensitivity/PPV to primary brain tumors to be 58%/92% and to brain metastases 48%/100%.

Similarly to the calculation presented above for the TRAMs, the percentage of high rCBV volumes within the enhancing ROIs in the presurgical maps was compared with the percentage of active tumor in the histological samples. The correlation

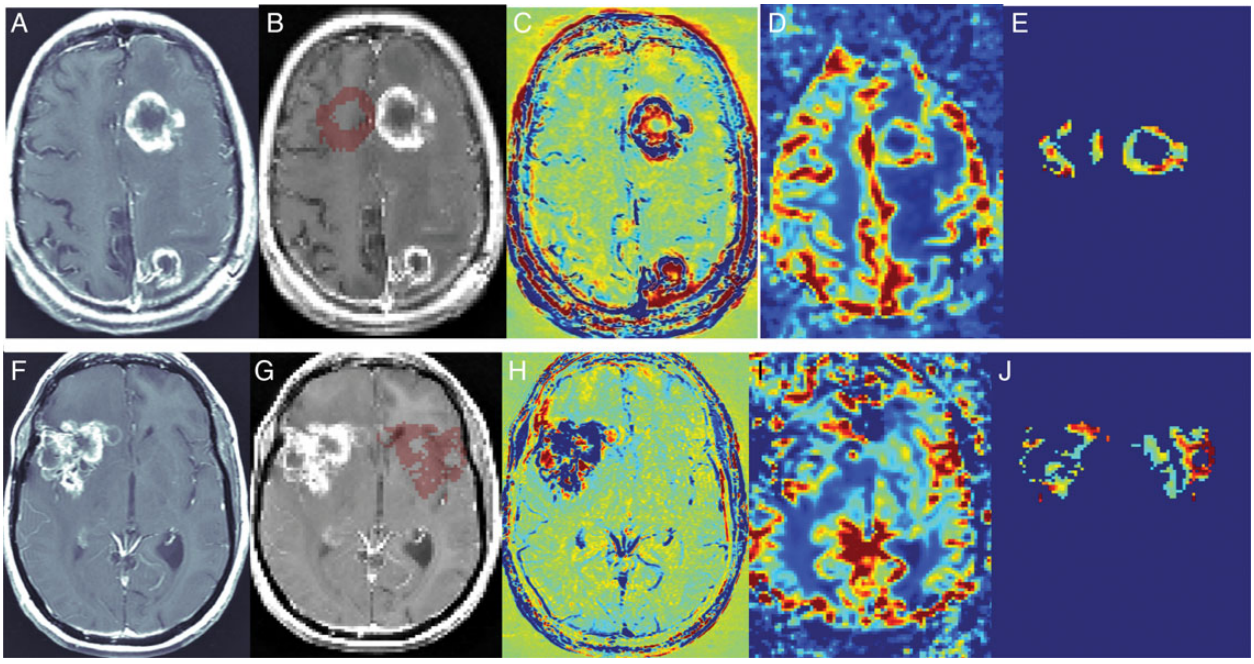

Fig. 3. Examples of a patient with a NSCLC metastasis (A–E) determined by the study neuroradiologist to have high rCBV (tumor) and a GBM patient (F–J) determined to have moderate rCBV (no tumor). Both lesions were resected and found to consist of active tumor. Shown are contrast-enhanced T1-weighted MRIs (A and F), MRIs with the contralateral ROI in red (B and G), the calculated TRAMs (C and H), the calculated rCBV maps (D and I), and the pixels of high rCBV within the enhancing ROI and the contralateral ROI (E and J). ROI analysis of the metastasis showed that 72% of the enhancing ROI consisted of high rCBV, and average rCBV in the enhancing ROI was 2.3 ± 1.1. In the contralateral ROI (red mask, B) 57% of the ROI showed high rCBV, and average rCBV was 2.3 ± 1.1 as well. ROI analysis of GBM showed that 47% of the enhancing ROI consisted of high rCBV, and average rCBV was 2.0 ± 1.3. In the contralateral ROI 67% of the ROI showed high rCBV, and average rCBV was 2.6 ± 1.5. The masking effects of normal brain vasculature are reflected in these examples by the similarity of the ipsi- and contralateral ROI analysis results. The clinical approach, on the other hand, identified the metastasis as tumor and the GBM as nontumor.

was calculated for 8 samples that had rCBV data available, resulting in no correlation: $r^2 = 0.01$, $P < .84$.

New Lesions Discovered During Follow-up

Twenty-four new metastases were discovered in 15 patients with brain metastases and 1 patient with atypical meningioma during their participation in the study. Twenty-three of the new lesions were small (<1 cm) and all showed a solid blue volume on the TRAMs. One lesion was larger (~2 cm in diameter) and cystic with a blue rim. None of these tumors showed high rCBV.

Potential Application of Treatment Response Assessment Maps for Improved Patient Management

Overall, 492 maps were calculated for 150 patients during their participation in the study. Once the TRAMs are validated to reliably depict tumor burden, and therefore also changes in tumor burden, they may be used to provide essential information for improved patient management. Detailed examples demonstrating the potential application of the TRAMs to the daily management of brain tumor patients can be found in Supplementary File 2.

Potential application of the TRAMs for differentiating progression from treatment effects in brain tumors posttreatment is demonstrated in the case of patient #3. In this case, significant increase in the blue/tumor volume in the TRAMs was indicative of progression. The patient was resected, and histology confirmed active tumor (Supplementary Figs S1 and S2). The same application is also demonstrated in the cases of patients #30 and #1, where the TRAMs favored pseudoprogression over progression, and in the case of patient #25, where the TRAMs favored radiation necrosis over progression (Supplementary Figs S3–S5).

The potential application of the TRAMs for assessing the existence/absence of residual tumor postsurgery is demonstrated in the case of patient #18 (Supplementary Figs S6 and S7), showing residual tumor 1 month after a first surgery and 10 days after a second surgery, and of patient #3 (Supplementary Fig. S1F), where the TRAMs favored postsurgical changes over residual tumor.

The potential application of the TRAMs for differentiating malignant transformation from treatment effects in low-grade tumors is demonstrated in the case of patients #50 and #61 (Supplementary Fig. S8). The TRAMs depicted blue lesions favoring malignant transformation over treatment effects as confirmed by the following histology (patient #50) and continued progression (patient #61).

The low sensitivity of the TRAMs to susceptibility artifacts leads to an additional potential application of depicting active tumor within hemorrhages as demonstrated in Supplementary Fig. S9.

Discussion

Conventional MRI is unable to differentiate progression from treatment effects. The TRAMs are similar to DSC-MRI in the sense that they are based on vascular function, but they apply an entirely different concept, long delays, which is highly sensitive to the difference between tumor and treatment effects. Unlike the model-dependent DSC-MRIs, which assess vessel function during the first contrast bolus, our technique is model independent. The novel finding that at long delays there are only 2 opposite options, contrast clearance versus contrast accumulation, with no overlap between the 2, is the reason this methodology has the potential of providing a simple/robust solution for differentiating tumor from treatment effects in a variety of neuro-oncological settings.

Since DSC-MRI is the most studied methodology in this context, all patients were scanned by DSC-MRI. We analyzed the DSC-MRI data using 2 approaches, ROI analysis and the clinical approach. ROI analysis was applied to a subgroup of 46 resected lesions. Despite the fact that 44 of the 46 lesions showed active tumor in histology, neither the average rCBV value nor the high rCBV volume showed significant difference between the enhancing ROIs and the contralateral ROIs. These results suggest that rCBV of the tumors is heavily masked by rCBV of normal brain vasculature. No correlation was found between the percentage of high rCBV and the percentage of active tumor in a small cohort of 8 lesions resected en bloc. This result may be explained by the small number of lesions and does not rule out the clinical application of rCBV, whose values tend to vary significantly within the tumor region (Figs 1 and 3). When using the clinical approach, even a small percentage of high rCBV within the enhancing region is an indication of tumor, thus providing essential information for decision making.

Therefore, we also applied the clinical approach to rCBV, yielding sensitivity/PPV of 51%/96%. In the case of the TRAMs, normal brain is depicted as a flat green background with no masking effects, and therefore both ROI analysis and clinical evaluation can be easily applied.

The sensitivity of rCBV (clinical approach) to tumor was 51% using a cohort of 46 resected patients. Using the same cohort, the sensitivity of rCBV to blue regions in the TRAMs was similar (48%). Still, the sensitivity of rCBV to blue regions in the TRAMs in a larger cohort of patients (215 TRAMs calculated for patients presenting with a question of tumor vs treatment effects) was 23%. This number is significantly lower than the sensitivity to both tumor and blue regions in the TRAMs determined using the cohort of resected patients. One explanation may be bias of the resected-lesion group toward larger lesions. Since rCBV is less sensitive to small lesions, which are usually not resected, the sensitivity determined using the resected cohort may be overestimated. For example, none of the 24 new metastases discovered during follow-up were resected and none had high rCBV.

A potential limitation of our DSC-MRI analysis is the lack of preload dosing to correct for T1 leakage effects, which could affect rCBV values and accuracy.[34,35] Additional recently presented leakage correction software methods[13,36–38] could also affect rCBV values and accuracy.

It is important to note that reliable determination of histological tumor burden is challenging, especially in lesions containing macroscopic necrotic/hemorrhagic regions. In many cases tissues are lost during the surgery and/or during handling/fixation/slicing of the samples. Therefore, we studied the correlation with tumor burden only in cases where it could be reliably assessed: in lesions resected en bloc or showing no tumor.

In order to provide the clinicians with a new diagnostic tool, it is essential to reach high PPV. Relative cerebral blood volume satisfies this requirement (96% in our cohort), and therefore, despite its low sensitivity, rCBV has been widely used. In our study, all cases showing high rCBV also showed a blue component in the TRAMs, consistent with the high PPV of both methods. A major advantage of the TRAMs over DSC-MRI is the high sensitivity to active tumor, reaching above 90%.

Another advantage of the long delays is the ability to use robust imaging sequences, resulting in high resolution maps with high sensitivity to small changes and low sensitivity to susceptibility artifacts. The importance of the latter is also demonstrated in the TRAMs' ability to detect active tumor within hemorrhages while rCBV remains low.

In a previous study including 34 patients with ischemic stroke, only red regions were depicted in the maps.[39] In the current study, 24 new/untreated lesions were discovered during follow-up, all blue in the maps. Both groups further establish the association of blue with active tumor and red with nontumor regions.

An unavoidable drawback of the TRAMs is the requirement to wait >1 h after contrast injection. To reduce patient inconvenience and avoid wasting expensive MRI time, our patients were let out of the machine after the conventional MRI exam while other patients were scanned. Our patients were then returned to the scanner for the delayed MRIs.

In summary, the TRAMs present a novel model-independent approach providing efficient separation between tumor/nontumor tissues by adding a short T1-MRI scan >1 h post contrast injection. The methodology uses robust acquisition sequences, which may be acquired on any MRI system with conventional types/doses of contrast agents, providing high resolution maps with minimal sensitivity to susceptibility artifacts. In most hospitals, clinical decisions whether to operate, change treatment, or continue treatment are made by an interdisciplinary team of physicians who are often unable to reach a unanimous decision due to the uncertainty in radiological interpretation. The TRAMs, shown here to provide a reliable assessment of tumor burden, may change this situation into clear/objective and unanimous decisions.

Supplementary Material

Supplementary material is available online at *Neuro-Oncology* (http://neuro-oncology.oxfordjournals.org/).

Funding

This work was supported by a KAMIN grant (#49745) from the Israeli Ministry of Industry and Commerce, by a generous donation from Roche Pharmaceuticals and by the Joseph Sagol PhD scholarship for Dianne Daniels.

Acknowledgments

The authors thank Prof Ram for many fruitful discussions and Drs Grossman, Nechushtan, Spector, and Jonas and Prof Siegal for referring patients to the study. Special thanks to the neuropathologists Dr Kanianu and Dr Fichman for fruitful discussions regarding pathological finding. This work was performed in partial fulfillment of the requirements for a PhD degree of Dianne Daniels, Sackler Faculty of Medicine, Tel Aviv University, Israel.

Conflict of interest statement. Authors L.Z., D.G., D.L., D.D., and Y.M. are inventors on pending patents.

References

1. Brandsma D, Stalpers L, Taal W, et al. Clinical features, mechanisms, and management of pseudoprogression in malignant gliomas. *Lancet Oncol*. 2008;9(5):453–461.
2. Brandsma D, van den Bent MJ. Pseudoprogression and pseudoresponse in the treatment of gliomas. *Curr Opin Neurol*. 2009;22(6):633–638.
3. Chamberlain MC, Glantz MJ, Chalmers L, et al. Early necrosis following concurrent Temodar and radiotherapy in patients with glioblastoma. *J Neurooncol*. 2007;82(1):81–83.
4. Chaskis C, Neyns B, Michotte A, et al. Pseudoprogression after radiotherapy with concurrent temozolomide for HGG: clinical observations and working recommendations. *Surg Neurol*. 2009; 72(4):423–428.
5. de Wit MC, de Bruin HG, Eijkenboom W, et al. Immediate post-radiotherapy changes in malignant glioma can mimic tumor progression. *Neurology*. 2004;63(3):535–537.
6. Fink J, Born D, Chamberlain MC. Pseudoprogression: relevance with respect to treatment of HGGs. *Curr Treat Options Oncol*. 2011; 12(3):240–252.
7. Sanghera P, Rampling R, Haylock B, et al. The concepts, diagnosis and management of early imaging changes after therapy for glioblastomas. *Clin Oncol*. 2012;24(3):216–227.
8. Taal W, Brandsma D, de Bruin HG, et al. Incidence of early pseudoprogression in a cohort of malignant glioma patients treated with chemoirradiation with temozolomide. *Cancer*. 2008; 113(2):405–410.
9. Lawrence YR, Li XA, el Naqa I, et al. Radiation dose-volume effects in the brain. [review]. *Int J Radiat Oncol Biol Phys*. 2010;76(3 Suppl):S20–S27.
10. Tihan T, Barletta J, Parney I, et al. Prognostic value of detecting recurrent glioblastoma multiforme in surgical specimens from patients after radiotherapy: should pathology evaluation alter treatment decisions? *Hum Pathol*. 2006;37(3):272–282.
11. Forsyth PA, Kelly PJ, Cascino TL, et al. Radiation necrosis or glioma recurrence: is computer-assisted stereotactic biopsy useful? *J Neurosurg*. 1995;82(3):436–444.
12. Perry E, Schmidt RE. Cancer therapy–associated CNS neuropathology: an update and review of the literature. *Acta Neuropathol*. 2006;111(3):197–212.
13. Hu LS, Eschbacher JM, Heiserman JE. Reevaluating the imaging definition of tumor progression: perfusion MRI quantifies recurrent glioblastoma tumor fraction, pseudoprogression, and radiation necrosis to predict survival. *Neuro-Oncol*. 2012;14(7): 919–930.
14. Jahangiri A, Aghi MK. Pseudoprogression and treatment effect. *Neurosurg Clin N Am*. 2012;23(2):277–287.
15. Rane N, Quaghebeur G. CNS effects following the treatment of malignancy. *Clin Radiol*. 2012;67(1):61–68.
16. Shaw E, Scott C, Souhami L, et al. Single dose radiosurgical treatment of recurrent previously irradiated primary brain tumors and brain metastases: final report of RTOG protocol 90-05. *Int J Radiat Oncol Biol Phys*. 2000;47(2):291–298.
17. van den Bent MJ, Vogelbaum MA, Wen PY, et al. Endpoint assessment in gliomas: novel treatments limit the usefulness of the classical Macdonald criteria. *J Clin Oncol*. 2009;27(18): 2905–2908.
18. Wen PY, Macdonald DR, Reardon DA, et al. Updated response assessment criteria for HGGs: response assessment in neuro-oncology working group. *J Clin Oncol*. 2010;28(11): 1963–1972.
19. Horská A, Barker PB. Imaging of brain tumors: MR spectroscopy and metabolic imaging. *Neuroimaging Clin N Am*. 2010;20(3): 293–310.
20. Tsuyuguchi N, Takami T, Sunada I, et al. Methionine PET for differentiation of recurrent brain tumor and radiation necrosis after SRS in malignant glioma. *Ann Nucl Med*. 2004;18(4): 291–296.
21. Nelson SJ. Assessment of therapeutic response and treatment planning for brain tumors using metabolic and physiological MRI. *NMR Biomed*. 2011;24(6):734–749.
22. Lacerda S, Law M. MR perfusion and permeability imaging in brain tumors. *Neuroimaging Clin N Am*. 2009;19(4):527–557.
23. Mills SJ, Soh C, O'Connor JP, et al. Enhancing fraction in glioma and its relationship to the tumoral vascular microenvironment: a dynamic contrast-enhanced MRI study. *Am J Neuroradiol*. 2010; 31(4):726–731.
24. Aronen HJ, Perkiö J. Dynamic susceptibility contrast MRI of gliomas. *Neuroimaging Clin N Am*. 2002;12(4):501–523.
25. Covarrubias DJ, Rosen BR, Lev MH. Dynamic MR perfusion imaging of brain tumors. *Oncologist*. 2004;9(5):528–537.
26. Gasparetto EL, Pawlak MA, Patel SH, et al. Posttreatment recurrence of malignant brain neoplasm: accuracy of rCBV in discriminating low from high malignant histologic volume fraction. *Radiology*. 2009;250(3):887–896.
27. Hu LS, Baxter LC, Smith KA, et al. rCBV values to differentiate high-grade glioma recurrence from posttreatment radiation effect: direct correlation between image-guided tissue histopathology and localized DSC-PWI measurements. *Am J Neuroradiol*. 2009;30(3):552–558.
28. Kim YH, Oh SW, Lim YJ, et al. Differentiating radiation necrosis from tumor recurrence in high-grade gliomas: assessing the efficacy of 18F-FDG PET, 11C-methionine PET and perfusion MRI. *Clin Neurol Neurosurg*. 2010;112(9):758–765.
29. Mangla R, Singh G, Ziegelitz D, et al. Changes in rCBV 1 month after radiation temozolomide therapy can help predict overall survival in patients with glioblastoma. *Radiology*. 2010;256(2):575–584.
30. Sugahara T, Korogi Y, Tomiguchi S, et al. Posttherapeutic intraaxial brain tumor: the value of perfusion-sensitive contrast-enhanced MRI for differentiating tumor recurrence from nonneoplastic contrast-enhancing tissue. *Am J Neuroradiol*. 2000;21(5): 901–909.
31. Young RJ, Gupta A, Shah AD, et al. MRI perfusion in determining pseudoprogression in patients with glioblastoma. *Clin Imaging*. 2013;37(1):41–49.

32. Zach L, Guez D, Last D, et al. Delayed contrast extravasation MRI for depicting tumor and non-tumoral tissues in primary and metastatic brain tumors. *PLoS One*. 2012;7(12):e52008.
33. Young RJ, Akash AG, Shah D. MRI perfusion in determining pseudoprogression in patients with glioblastoma. *Clin Imag*. 2013;37(1):41–49.
34. Hu LS, Baxter LC, Pinnaduwage DS, et al. Optimized preload leakage-correction methods to improve the diagnostic accuracy of dynamic susceptibility-weighted contrast-enhanced perfusion MR Imaging in posttreatment gliomas. *Am J Neuroradiol*. 2010; 31(1):40–48.
35. Boxerman JL, Schmainda KM, Weisskoff RM. Relative cerebral blood volume maps corrected for contrast agent extravasation significantly correlate with glioma tumor grade, whereas uncorrected maps do not. *Am J Neuroradiol*. 2006;27(4):859–867.
36. LaViolette PS, Cohen AD, Prah MA, et al. Vascular change measured with independent component analysis of dynamic susceptibility contrast MRI predicts bevacizumab response in high-grade glioma. *Neuro Oncol*. 2013;15(4):442–450.
37. Emblem KE, Bjornerud A, Mouridsen K, et al. T1- and T2 *-dominant extravasation correction in DSC-MRI: Part II—predicting patient outcome after a single dose of cediranib in recurrent glioblastoma patients. *J Cereb Blood Flow Metab*. 2011;31(10):2054–2064.
38. Sorensen AG, Emblem KE, Polaskova P, et al. Increased survival of glioblastoma patients who respond to antiangiogenic therapy with elevated blood perfusion. *Cancer Res*. 2012;72(2):402–407.
39. Israeli D, Tanne D, Daniels D, et al. The application of MRI for depiction of subtle BBB disruption in stroke. *Int J Biol Sci*. 2010; 7(1):1–8.